A new approach to highly resolved measurements of turbulent flow

To cite this article: J Puczylowski *et al* 2015 *Meas. Sci. Technol.* **26** 055302

View the article online for updates and enhancements.

A new approach to highly resolved measurements of turbulent flow

J Puczylowski[1], **A Hölling**[1], **J Peinke**[1], **R Bhiladvala**[2] **and M Hölling**[1]

[1] Institute of Physics, ForWind, University of Oldenburg, Ammerländer Herrstr. 136, Oldenburg, Germany
[2] University of Victoria, 3800 Finnerty Rd, Victoria, BC V8P 5C2, Canada

E-mail: jaroslaw.puczylowski@forwind.de

Abstract

In this paper we present the design and principle of a new anemometer, namely the 2d-Laser Cantilever Anemometer (2d-LCA), which has been developed for highly resolved flow speed measurements of two components (2d) under laboratory conditions. We will explain the working principle and demonstrate the sensor's performance by means of comparison measurements of wake turbulence with a commercial X-wire. In the past we have shown that the 2d-LCA is capable of being applied in liquid and particle-laden domains, but we also believe that other challenging areas of operation such as near-wall flows can become accessible.

(Some figures may appear in colour only in the online journal)

1. Introduction

Turbulence plays a key role in many fields of application, e.g. it is of great importance for various processes, such as combustion or mixing. The characterization of turbulent flows by itself is still a major challenge for researchers and engineers. Computer-based simulations have become a powerful tool for investigating turbulent flows. However, despite continuously increasing computational power, direct numerical simulations (DNS) of the Navier–Stokes equations (NSE) fail for turbulent flows with very large Reynolds numbers. Until now the DNS computation with the highest Re_λ of 1130 has been achieved by [25]. Apart from DNS, various other tools in the field of computational fluid dynamics (CFD) exist. A very common approach is the transformation of the NSE into the so-called Reynolds averaged Navier–Stokes equations (RANS), which include a second-order tensor (Reynolds stress tensor). However, all CFD approaches and even the NSE itself remain

models and need to be validated by experimental data. It is therefore important to carry forward the development and optimisation of experimental techniques as well.

The evaluation of the measurement data of turbulent flows is accomplished by means of stochastic methods. This is the only reasonable approach as turbulent flows are unrecoverable in their totality and are also irregular in time and space. In order to investigate the properties of turbulent flows, some demands are placed on the anemometers. One key parameter is the resolution power, which specifies the depth of insight into the turbulent flow. In particular, the total resolution power depends on the ability of resolving spatial structures and temporal dynamics. There are various different sensors for the characterization of turbulent flows [19]. For atmospheric turbulence cup anemometers or ultrasonic anemometers are often used. Both anemometers measure with a temporal resolution in the order of Hz and feature spatial resolutions of about 10 cm.

For laboratory-generated turbulence, in which the investigation of small scales is desired, much higher resolutions are needed. As a consequence of Re being much smaller under laboratory conditions compared to the atmosphere, and the ratio of the integral length and Kolmogorov length scaling

Figure 1. Illustration of the 2d-Laser Cantilever Anemometer with a detailed view of the cantilever.

with $L/\eta \sim Re^{3/4}$ (L is usually fixed by the experimental setup), a high spatial resolution for resolving all the relevant scales is necessary.

Highly resolved measurements under laboratory conditions are often accomplished using hot-wire anemometers. These sensors use a tiny platinum or tungsten wire as the crucial sensor element. The wire is heated by means of electrical current and is then brought into the flow. The flow circulation affects the temperature of the wire and thus changes its electrical resistance. When operating in CTA mode (constant temperature anemometry), the current needed in order to maintain a constant temperature is directly connected to the flow velocity, and thus serves as the measuring signal. Hot-wire probes with a single wire for one-dimensional measurements yield temporal resolutions of tens of kHz (depending on various parameters such as the overheat-ratio or material properties) and spatial resolutions in the millimeter range (length of wire). Shorter probes become very fragile as the diameter to length ratio of about 1 : 200 must be maintained in order to minimize heat conduction to the prongs, which in turn causes a decrease in sensitivity [20]. For directional measurements in two dimensions X-wires exist. For X-wires the resolution is limited by the spacing between the wires and the wire lengths. A certain spacing between the wires is necessary in order to avoid temperature cross talk.

Although hot-wire anemometry is widely accepted, there are some underlying restrictions. For instance, due to the measuring principle hot wires cannot be used for measurements in conductive or particle-laden fluids [1, 4]. Hot wires are also not suitable for measurements carried out very close to walls, since the heat reflection might have an impact on the measuring signal [5, 6]. Even conventional hot-wire-based wall shear stress sensors, which are embedded in the surface, deliver a poor signal quality due to unwanted heat conduction to the surface [13]. A detailed study of the dynamic response of elevated and flush-mounted hot wires with regard to the wall distance, the type of wall substrate and convective velocity is given in [22, 23][3]. For hot wires the relation of the measuring signal versus inflow velocity follows King's Law [20], in which velocity v is related to voltage E as $v \approx E^4$. Thus, the resolution power decreases with higher flow velocities.

Aside from restrictions on the areas of operation, hot wires show other disadvantages. The non-shielded wires, which are
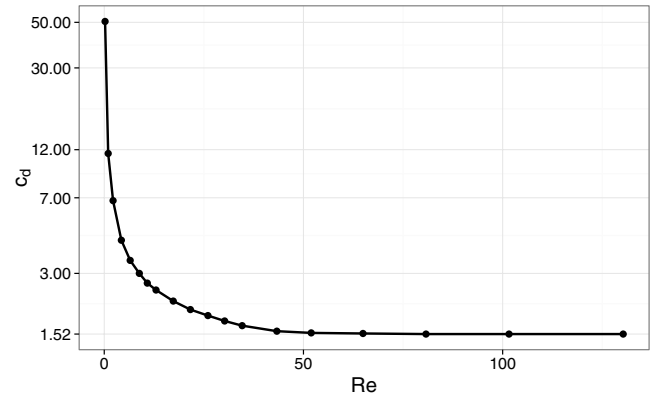
Figure 2. Variation of c_d with respect to Re.

part of an amplification circuit, act as antennas, and are thus susceptible to electromagnetic interference [1, 4]. Moreover, X-wires typically perform measurements for inflow angles of about ± 40° only. Angles of attack that exceed this range are interpreted incorrectly. This is because the calibration plane of X-wires collapses and loses its uniqueness for large inflow angles. Lastly, since the smallest changes in wire tension caused by ambient temperature fluctuations or wire aging likely have an impact on the heat dissipation, the X-wires need to be recalibrated very often.

For these reasons we have developed a new kind of sensor, the so-called Laser Cantilever Anemometer [4]. Its measuring principle is adopted from atomic force microscopes where the deformation of a tiny beam (cantilever) is gathered using the laser lever arm principle. The cantilever used for the 2d-LCA acts like a flow body and experiences a deformation due to the moving medium, i.e. wind flow. The first prototype of the LCA was capable of performing measurements of one velocity component only. Later, in [1] the first two-dimensional LCA (2d-LCA) with an angular range comparable to X-wires was introduced.

In this paper we focus on our newest version of the 2d-LCA. It features a new design of the cantilever, revised electronics and an overall improved setup. The angular range has been further increased to inflow angles of ± 90° at spatial and temporal resolutions comparable to X-wires. The new 2d-LCA is shown in figure 1.

2. Method

2.1. Measuring principle

The measuring principle applied for the 2d-LCA is adopted from atomic force microscopy (AFM). In atomic force microscopes a probe tip, which is attached to the forefront of a tiny cantilever, is used to measure the surface depth of a sample. For this purpose the atomic force, i.e. the distance between the tip and the sample surface are maintained constant. The z-displacement of the cantilever changes in accordance with the topography of the surface and is monitored by means of the laser pointer principle. To do so, a laser beam is focused on the top surface of the cantilever. It produces a reflection spot that moves subject to the displacement of the cantilever

---

[3] We want to emphasize that only the measuring principle and not the implementation as presented in the following might be feasible for measurements of near-wall flows.

[4] This only is true for deflections within the elastic range, i.e. the amount of deflection where the stiffness remains constant.
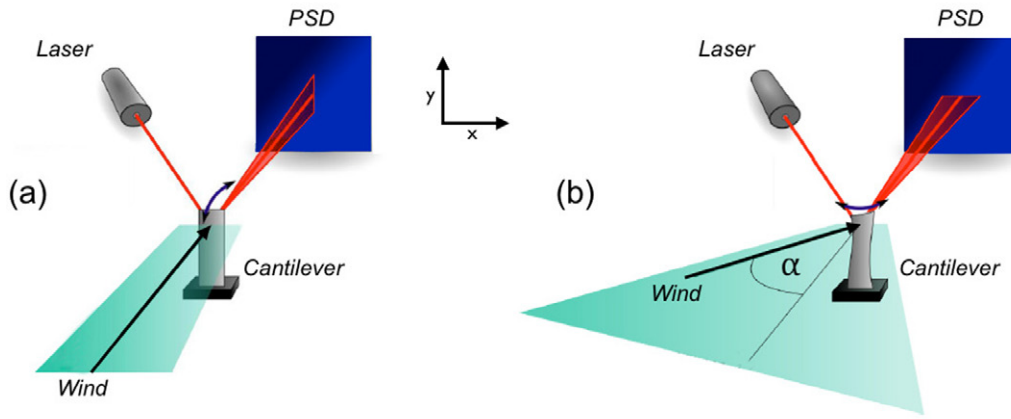
Figure 3. Schematic illustration of the bending (*a*) and twisting (*b*) of the cantilever.

and is tracked using a position sensitive detector (PSD). The position of the reflection spot along the PSD contains the deflection information of the cantilever and thus serves as the measuring signal.

The same principle is applied for the 2d-LCA. Here the cantilever itself and not a specially designed tip is the sensing element. It has typical dimensions of $160 \times 40 \times 1.6$ μm (length $\times$ width $\times$ thickness). The cantilever is made of silicon and is coated with a reflective material (aluminium) at its tip. It is attached to the forefront of the sensor and is brought into the flow where it experiences the drag force F_{drag}. For a straight inflow $\widehat{F}_{\text{drag}}$ is given by:

$$\widehat{F}_{\text{drag}} = \frac{1}{2} \cdot c_d(v) \cdot \rho \cdot A \cdot v^2. \tag{1}$$

Here c_d is the drag coefficient of the cantilever, A is the area of the large surface of the cantilever for this bluff body flow, ρ is the density of the fluid and v is the flow velocity. The small dimensions of the cantilever imply low local Reynolds numbers (about 50 for typical laboratory flow velocities of ≈ 20 m s^{-1}). The dependence of Re upon c_d has been studied using steady-state CFD simulations performed with OpenFOAM. It has been found that c_d for a one-sidedly fixed cantilever undergoes large variations of Re up to about 40 and converges to a constant value of 1.52 for a higher Re, as can be seen in figure 2. The divergence from literature values of $c_d = 1.19$ (rectangular plate of length/width ratio $4:1$ for Re of $100\text{--}100\,000$ [11, 12]) is caused by different boundary conditions that apply to free-hanging structures. For constant ρ and $v \gtrsim 1$ m s^{-1} the variation of c_d/v is small compared to v^2, and therefore one can assume $\widehat{F}_{\text{drag}} \propto v^2$. This also means that the deflection of the cantilever and hence the resolution power of the sensor increase with increasing v^4.

For oblique inflows the cantilever experiences an additional transverse force, which results in a twisting deformation. Therefore, the deformation of the cantilever due to the total drag force F_{drag} can be taken as a superposition of bending and twisting. The deflection of the reflecting laser spot along the PSD element due to this twisting is perpendicular to the deflection that corresponds to simple bending (figure 3).

In order to capture both deflections, a two-dimensional PSD element (2d-PSD) of type Hamamatsu S5990 is used. In this manner the longitudinal and transverse velocity components can be measured simultaneously. The current signals from the 2d-PSD are processed using an analog computation and amplification circuit. In general one could also use cantilevers in tapping mode in order to measure flow velocities [9]; however, this approach does not allow for directional measurements.

The deflection distance of the spot along the 2d-PSD can be estimated by calculating the cantilever deflection *s* at the tip by means of the classical beam theory. For a uniformly loaded cantilever beam of length *l* the maximum deflection becomes:

$$s(l) = \widehat{F}_{\text{drag}} \cdot \frac{l^3}{8 \cdot E \cdot I_{\text{A}}}, \tag{2}$$

with the Young's modulus E, which describes the relation between the tension and elongation of a material during deformation[5]. I_{A} is the moment of inertia of the area. As *s* is only proportional to the velocity squared of the flow ($s \propto \widehat{F}_{\text{drag}} \propto v^2$), all the other values remain constant.

The deflection angle γ of the cantilever at the center of the reflection pad, which corresponds to the length l_{pad} can be assessed according to:

$$\gamma = \arctan\left[\widehat{F}_{\text{drag}} \cdot \frac{l^3}{2E \cdot I_{\text{A}}} \left(\frac{l_{\text{pad}}^4}{12l^4} - \frac{l_{\text{pad}}^3}{3l^3} + \frac{l_{\text{pad}}^2}{2l^2} \right) \right]. \tag{3}$$

This deflection causes a displacement of the reflecting laser beam spot on the 2d-PSD of length $D = d \cdot \tan(\gamma)$ with $d = 60$ mm being the distance between the cantilever and the 2d-PSD. Thus, for a typical straight air stream of 15 m s^{-1} a deflection of the laser spot along the active area of 1.02 mm is expected, fitting well to the dimensions of the 2d-PSD of 4 mm $\times$ 4 mm.

2.2. Design of the sensor

The sensor body as shown in figure 1 is completely made of aluminium. All the components were anodized to improve

---

[5] Here the Young's modulus corresponding to the 100 layer (perpendicular to the bending line) is considered.
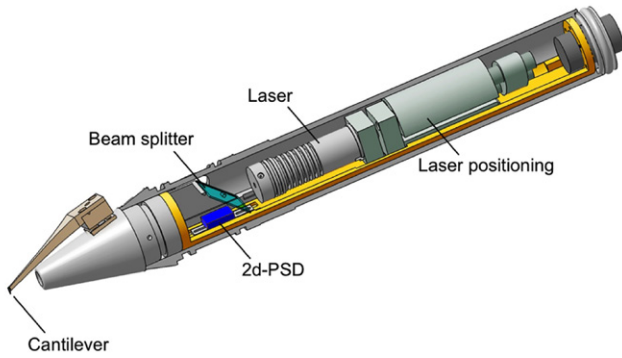
Figure 4. Schematic illustration of the 2d-LCA and its main components without the housing.

Figure 5. Illustration of the laser path within the 2d-LCA. The laser beam falls on the tip of the reflective cantilever surface and is reflected towards a 2d-PSD. A pellicle beam splitter is used in order to allow for a perpendicular incidence direction of the laser beam.
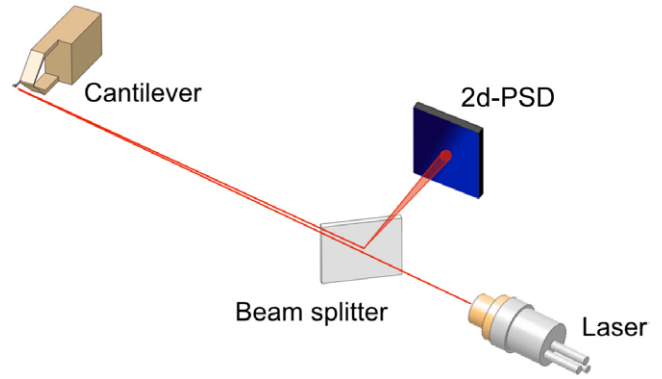
corrosion resistance. Furthermore, the sensor was designed to be waterproof and thus also allows for measurements in liquids [1]. The front face of the 2d-LCA was designed as conical with an opening angle of 24° in order to avoid an interaction between the sensor body and the flow that might influence the deflection of the cantilever [4]. The main parts of the sensor are schematically shown in figure 4.

The laser beam used for pointing onto the cantilever is provided by a power-controlled laser diode of type ADL-63054TA2 ($\lambda = 630$ nm, $P = 5$ mW), placed on a small positioning stage. The adjustment of the stage, i.e. the direction of the outgoing laser beam, is performed using two DC motors. This enables the laser to be adjusted remotely without opening the sensor housing. This is very useful in particular in situations where the sensor is aligned in a measuring setup with difficult access.

The laser beam is focused on the tip of the cantilever using a gradient index lens (GRIN-lens). Unlike conventional spherical lenses, GRIN-lenses have flat-end faces and a radial changing refractive index realizing a continuous cosine ray trace within the lens. The shape of the emerging beam mainly depends on the pitch length of the GRIN-lens. A pitch length of 1 corresponds to one complete cosine trajectory. For the 2d-LCA a GRIN-lens with a diameter of 1.8 mm and a pitch length of 0.16 is used. The big advantages of these lenses compared to spherical lenses are the almost non-existent spherical aberrations and the compact size [2].

The laser beam path within the sensor is illustrated in figure 5. The laser beam falls onto a customized pellicle beam splitter with a reflection to transmission ratio of 45/55. The transmitted part is guided towards the cantilever, whereas the reflected beam is not used. The returning beam (reflection from the cantilever) again crosses the beam splitter and finally falls on the active area of the 2d-PSD. Pellicle beam splitters are only a few μm thick and thus do not lead to unintended artifacts due to internal reflections which may cause ghost spots. In that way a more uniform reflective spot can be achieved as with conventional beam splitter plates or cubes.

The side of the cantilever facing the laser beam is equipped with a 40 μm × 40 μm pad at the tip coated with aluminium for good reflectivity, as light at 630 nm would simply pass through the silicon. The size of the reflection pad has a great influence on the signal quality. Figure 6 shows the different reflection spots when using a completely coated cantilever and a cantilever with a small reflective pad. Since the amount of deflection changes the cantilever's shape, especially in the section close to the built-in end, a completely coated cantilever causes a stronger distortion of the spot during deformation. This effect could cause an unintended change in light intensity distribution within the spot that would be interpreted by the 2d-PSD as a position change besides the real deflection. By contrast, the spot produced by the cantilever with a reflective pad remains largely constant. Furthermore, the spot is smaller and symmetric.

One phenomenon that always appears when using the laser pointer principle in connection with tiny sensing elements is diffraction. Some specially designed cantilevers (interdigitated cantilevers) even exploit this effect in a targeted way in order to precisely measure the deformation [10]. However, in the case of the measuring principle used here, diffraction is not desired. In fact, the performance of the 2d-PSD strongly depends on the size of the diffraction pattern accompanied by the reflection spot. Therefore, the spot size is an important design parameter for the sensor and needs to be considered carefully [16]. The intensity distribution of the diffraction pattern is given by:

$$I_\phi = I_S \cdot \text{sinc}^2(\pi \frac{w}{\lambda} \cdot \sin(\phi)), \tag{4}$$

with the width of the cantilever w, the diffraction angle ϕ and the wave length of the laser λ. The intensity distribution on the 2d-PSD for a cantilever of width $= 40$ μm at a distance of 6 cm is shown in figure 7. One can see that the main reflection and the 1st order diffraction completely fit onto the active area. The 2nd order diffraction falls onto the edge; however, its light intensity is only 1/60 of the total intensity. Still, once it moves outside and thus leaves the active area, it will lead to a change in the center of gravity of the total light intensity, which is interpreted by the 2d-PSD as a movement in the opposite direction. This effect, however, is very small and we neglect it if only light intensities due to higher order diffractions leave the active area. In the future one might think about applying a numerical correction or installing a larger 2d-PSD.
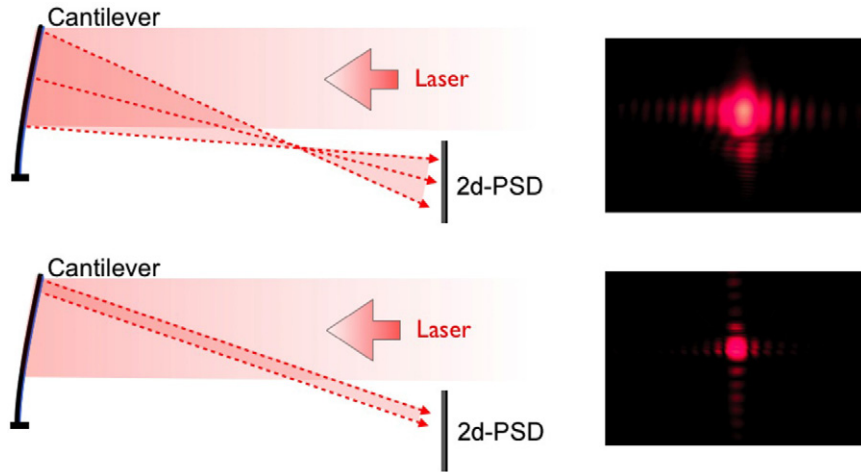
Figure 6. Illustration of the laser spots produced by a fully coated cantilever (top) and a cantilever partially coated at the tip (bottom).
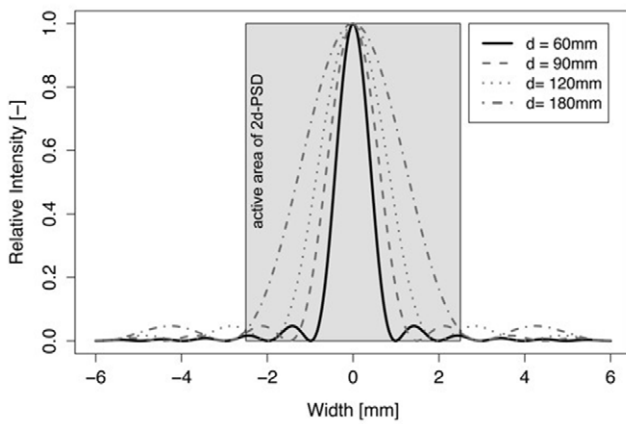
Figure 7. Intensity distribution of the diffraction pattern along the active area of the 2d-PSD for various distances between the cantilever and 2d-PSD. The calculation was carried out using a cantilever of width = 40 μm and λ = 630 nm. The main reflection order is normalized to 1.
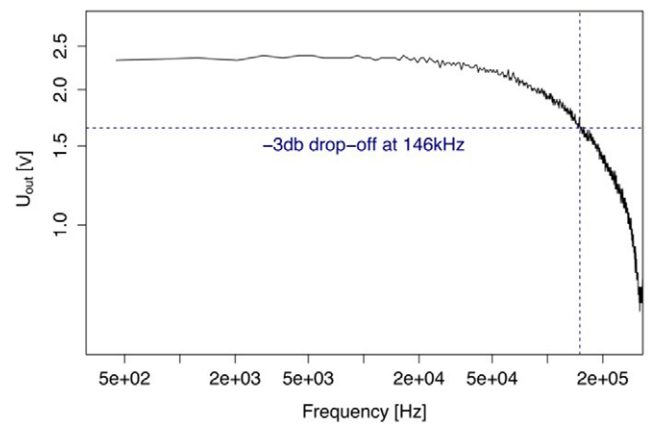
Figure 8. The graph represents the voltage output x of the electronics for a sinusoidal excitation at I_1 in the range of 500 Hz–250 kHz. The other three inputs of the electronics (I_2, I_3, I_4) are fed with constant DC-signals. The dashed lines correspond to a −3 dB decay in gain with regard to the voltage output at 100 Hz. Therefore, the cut-off frequency is about 146 kHz.

The 2d-LCA is equipped with a pin-cushion 2d-PSD. These PSDs have a low dark current noise and show better linearity when compared to tetra-lateral types. The light spot on the active area that is caused by the reflection of the laser produces some photocurrent. The total amount of this photocurrent is split up in accordance with the distance of the four electrodes at the corners of the active area. A change in any direction of the spot along the active area also changes the ratio of the currents. For further processing the current signals are transformed into voltage signals (I_1–I_4) by means of transimpedance circuits, and are then routed to analog operational amplifiers for the computation of the x- and y-positions of the center of gravity along the 2d-PSD according to:

$$x = \frac{I_1 + I_2 - (I_3 + I_4)}{\sum I_i} \tag{5}$$

$$y = \frac{I_1 + I_4 - (I_2 + I_3)}{\sum I_i} \tag{6}$$

The division by the sum of all 4 signals is used for right scaling independent of the total laser light intensity. The absolute position of the spot can be calculated by multiplying equations (5) and (6) by L/2.

For a faster response the 2d-PSD is operated using a positive bias voltage of 9 V at the common cathode. That way the depletion region of the active area is diminished. The cut-off frequency of the 2d-PSD, which corresponds to a −3 dB decay, is in the range of few MHz. In order to test the temporal response of the electronics, the amplifier gain of the output signals x and y was observed for a sinusoidal frequency sweep at the input I_1 from 500 Hz up to 250 kHz. During the sweep the remaining inputs I_2, I_3, I_4 remained constant. The amplitudes were chosen to match the range of voltages produced by the 2d-PSD in the trans-impedance circuit. As an example, the amplifier gain versus frequency sweep for the output of the x-component is shown in figure 8. The −3 dB cut-off occurs at a frequency of about f = 146 kHz. In principle this frequency can be increased even further, but for our purpose here of measuring flow velocities in the range
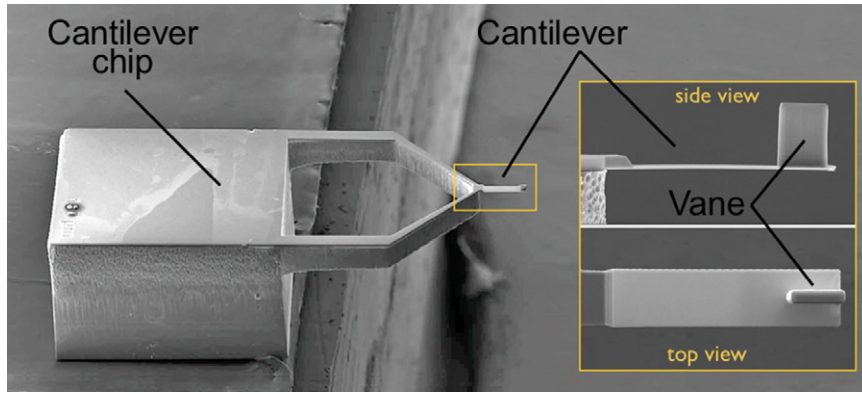
Figure 9. Cantilever chip captured with an electron microscope and a detailed view of the cantilever with vane.

of m s^{-1}, this corresponds to structure sizes that can be resolved of $u/f \approx 10$–$100\ \mu m$. These dimensions fit well to our design. A higher temporal resolution is not desired, as smaller structures would remain undetectable due to the size of the cantilever, but the principle of the 2d-LCA can be optimized further in this direction.

The 2d-LCA is connected to an external device by a 7-pin shielded data cable which contains a 16 bit A/D-converter (type Data Translation 9816) and a variable low pass filter for blanking high frequent noise and avoiding aliasing. Furthermore, it supplies the sensor with power and bears the controls for positioning the laser beam. The connection to a computer is done via USB.

2.3. Design of the cantilever

The silicon cantilever (figure 9) is the sensing element of the sensor. Its design is essential for the performance of the 2d-LCA. The whole cantilever chip is made using photolithography and etching processes. It consists of a device layer and a handle layer. Both layers are separated by a layer of silicon oxide of thickness 1 μm. The chip can be divided into three main segments: the supporting structure (handle layer) and the cantilever together with the vane (device layer). The supporting structure serves as the foundation for the cantilever in the first place. Its bottom side is also used as a contact area (approx. 0.8 mm × 1 mm) for its attachment to the mount. The shape of the supporting structure provides a stable foundation for the sensitive cantilever and allows for the low blockage of wind flow as discussed in [4]. Since the cantilever length is an important parameter in terms of the elastic deformation properties, various cantilever designs with different lengths ranging from 140–200 μm have been realized. Thus, different resolutions, depending on the requirements, can be achieved. However, all cantilevers have the same thickness of 1.6 μm and a width of 40 μm.

In order to increase the sensitivity towards cross winds, i.e. the amount of twisting, the tip on the inflow side is set up with an additional tiny vane (see figure 9). This structure is made of SU-8 (negative photo resist), a synthetic epoxy-like material, using deposition. The Young's modulus of post-baked SU-8 is >4 GPa. Structures made of SU-8 yield

aspect ratios of beyond 20. The two different vane designs were realized with dimensions 50 μm × 35 μm × 9 μm and 30 μm × 35 μm × 9 μm (height × length × width).

One very important property of the cantilever is its first natural frequency, i.e. the frequency of the first resonant mode. Because the cantilever is used as a sensing element in a turbulent flow, it must be ensured that the first natural mode cannot be excited by the flow itself. In laboratory generated turbulent airflows at moderate velocities below 20 m s^{-1}, frequencies above 20 kHz are unlikely to exist. Thus, the first natural frequency of the cantilever should be higher than this rough guide value.

An analytical approach for calculating the natural frequency of a rectangular cantilever of length l in vacuum is given by:

$$\omega_{\text{vac}} = \xi^2 \sqrt{\frac{EI_A}{m_s l^3}} = \sqrt{\frac{k}{m_s}}, \qquad (7)$$

with the first mode constant $\xi = 1.875$ for a clamped cantilevered beam, the Young's modulus E, the moment of inertia I_A and the spring constant $k = \xi^4 E I_A / l^3$. The quantity m_s denotes the structural mass of the cantilever. Using equation (7), the first undamped natural frequency of a simple cantilever (without vane) of length 140 μm is 102.5 kHz.

When operating under atmospheric pressure the surrounding flow can be taken to be in the continuum regime (Knudsen number Kn = 10^{-3}), and thus viscous effects need to be considered. However, a significant departure from ω_{vac} due to damping occurs only at low Q-factors of about $Q \approx 1$. In that case the damped resonant peak frequency for oscillation in a fluid is ω_{fluid}, calculated according to:

$$\omega_{\text{fluid}} = \left[\frac{k}{m} \left(1 - \frac{C^2}{2mk} \right) \right]^{\frac{1}{2}} \qquad (8)$$

Here $m = m_s + m_f$ is the effective mass with m_f being the fluid added mass seen by the oscillating cantilever when opposing the flow. Similarly, the total damping $C = C_s + C_f$ is the sum of the damping due to the structural composition C_s and fluid damping C_f. C_f and m_f for a beam with a rectangular cross-section can be calculated according to [15] by:
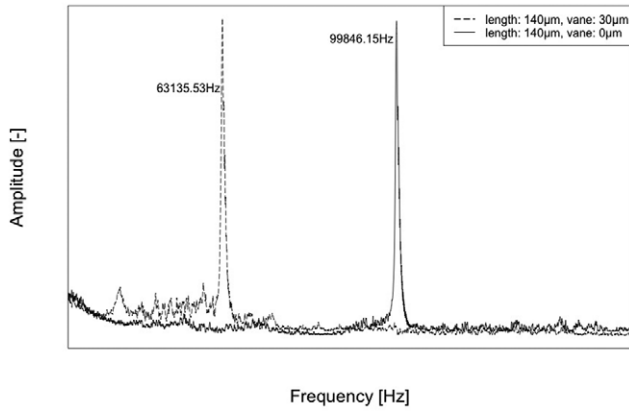
Figure 10. Sweep frequency of the excitation signal against the excitation amplitude of two different cantilevers. Dashed line: cantilever of 140 μm in length with vane of 30 μm in height; solid line: cantilever of 140 μm in length without vane.

$$m_f = \frac{\rho_f}{\rho_s} \kappa_m m_s \qquad (9)$$

$$C_f = \pi \nu \rho_f l \beta \kappa_c, \qquad (10)$$

with the dimensionless parameter $\beta = \omega \, w^2/4 \, \nu$, which depends on the kinematic viscosity ν, the width of the cantilever w and the undamped frequency ω and

$$\kappa_m = \mathrm{RE}\left(1 + \frac{4\mathrm{i}K_1(-\mathrm{i}\sqrt{\mathrm{i}\beta})}{\sqrt{\mathrm{i}\beta}\,K_0(-\mathrm{i}\sqrt{\mathrm{i}\beta})} \cdot \Omega(\omega)\right) \qquad (11)$$

$$\kappa_c = \mathrm{IM}\left(1 + \frac{4\mathrm{i}K_1(-\mathrm{i}\sqrt{\mathrm{i}\beta})}{\sqrt{\mathrm{i}\beta}\,K_0(-\mathrm{i}\sqrt{\mathrm{i}\beta})} \cdot \Omega(\omega)\right). \qquad (12)$$

K_0 and K_1 denote modified Bessel functions of the third kind and $\Omega(\omega)$ is a correction term needed for beams with rectangular cross-sections.

Next, we want to verify the analytically derived value of ω_{vac} for the cantilever without vane in an experiment and also to investigate the properties of a cantilever with vane. To do so, a setup originally developed for the characterization of nanowires, which are used as mass and force measurement devices [3], is used. The setup consists of a cantilever chip that is driven electrostatically in a vacuum chamber at 10^{-7} mbar. A sinusoidal sweep signal of 35–145 kHz and a constant amplitude of 2 mV provided by an Agilent E4402B spectrum analyzer, is used. The cantilever excitation is recorded using laser interferometry. Instead of using electrostatic excitation, one could also use magnetostrictive actuators, as presented in [8] or a piezo drive.

The responses of the cantilevers are shown in figure 10. The solid line graph corresponds to a simple cantilever of 140 μm in length and no vane. Its first natural frequency was measured and found to be 99.8 kHz. This value is close to the analytical estimate of 102.5 kHz (equation (7)).

The black graph represents the excitation of a cantilever of the same length but with a vane made of SU-8 with dimensions 30 μm × 40 μm × 9 μm (height × length × width). With
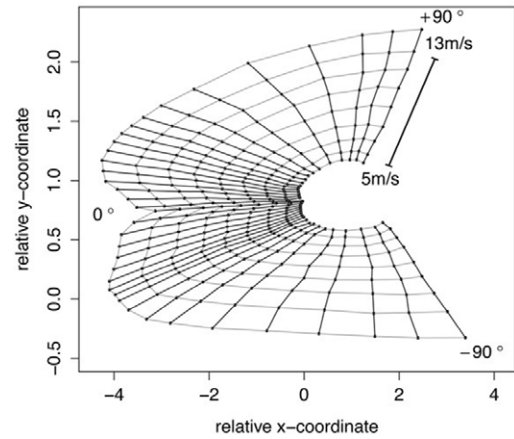
Figure 11. Example of a two-dimensional calibration plane of the 2d-LCA. The points represent the positions of the laser spot measured by the 2d-PSD element. The grey lines correspond to same velocities and the black lines to same angles of attack.

the additional mass of the vane, which is comparable to the mass of the cantilever, the natural frequency was found to decrease to 63.1 kHz (dashed line). An equally distributed additional mass of exactly the same magnitude as the mass of the cantilever would result in a decrease in the first natural frequency by a factor of $1/\sqrt{2}$, i.e. to ~70 kHz as can be seen from equation (7). Thus, a higher sensitivity towards cross winds by means of the vane is only achieved at the expense of temporal resolution. The highest operating frequency of the sensor should be less than the first resonant frequency.

The second important conclusion from the experimental investigation is that the first natural frequencies of both cantilevers are high enough to not interfere with the use of the cantilever deflection for sensing in turbulent flows under laboratory conditions. From the experiment carried out under a high vacuum, a Q-factor of $Q_s = 200$ was found for the cantilever without vane. Using the relation $C_s = m_s \omega_{\mathrm{vac}}/Q_s$ we can compute the expected Q-factor in a fluid at any resonance according to:

$$Q_f = Q_s \frac{\sqrt{1 + (m_f/m_s)}}{1 + (C_f/C_s)}, \qquad (13)$$

using equations (9)–(12). For air this approach leads to $Q_f = 6$, which is significantly smaller than Q_s. Therefore, even if the resonant modes of the cantilever were excited by the turbulent flow, the amplitude would be attenuated significantly by the strong damping.

2.4. Calibration

The calibration of the 2d-LCA is performed in a laminar flow wind tunnel, although the anemometer is applied to turbulence. This is because for typical laboratory flows at velocities around 20 m s^{-1} and Kolmogorov lengths η in the order of millimeters a quasi-static flow around the cantilever is assumed. The time needed for a flow structure of size η to pass the cantilever is about 50 μs, which is much slower than the time scales corresponding to the first resonant mode of the
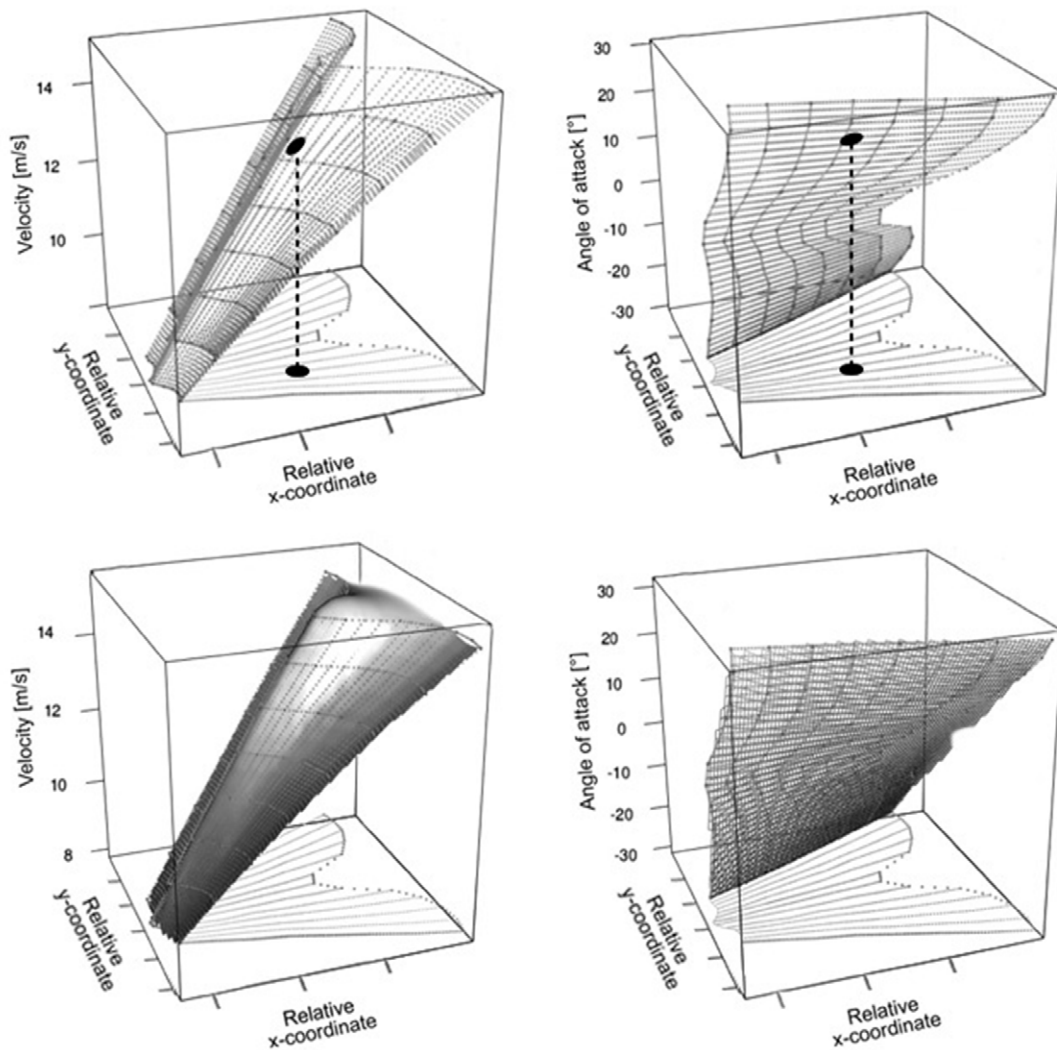
Figure 12. The 3D grids are obtained by plotting the relative positions of the laser spot against the inflow velocity and angle of attack. These grids can be refined by creating more grid points using 3D Akima spline functions (*top*). For the purpose of illustration the projection of one grid point onto the 2D calibration plane is shown. The Kriging algorithm is used to fit a surface to the grid (*bottom*).

cantilever. Therefore, in the above-mentioned case the cantilever faces laminar inflow only. Hence, non-linearities due to the dynamical response of the cantilever are not to be expected. However, as for any finite size, local probe limitations might occur for turbulent flows with smaller Kolmogorov lengths and/or faster mean velocities, i.e. for flow structures that pass the cantilever in a time close to $2\pi/\omega_{\text{fluid}}$. This event has not been studied yet and needs to be examined in the future.

During the calibration the relative coordinates of the spot along the 2d-PSD (equations (5) and (6)) are recorded for angles of attack ranging from $-90°$ to $+90°$ (relative to the cantilever) at intervals of typically $5°$ and velocities of $1–20$ m s^{-1} at intervals of 1 m s^{-1}. An example of a resultant calibration plane is illustrated in figure 11. For reasons of clarity, a velocity range of only $5–13$ m s^{-1} is shown.

The figure has a characteristic shape, in which the points corresponding to equal velocities form curved trajectories (indicated in grey) and the points corresponding to equal angles of attack are aligned along a straight line (indicated in black).

The calibration plane can easily be divided into two 3D graphs representing the relative coordinates against the flow velocities and the angles of attack. These graphs are shown in figure 12 (top) for a smaller segment of the calibration for reasons of clarity. The grid structures are refined by means of additional points, which were generated using 3D smooth spline functions. This step is necessary in order to ensure good prerequisites for a surface fit using the Kriging algorithm. The combination of both fitted surfaces (figure 12, bottom) allows for a straightforward allocation of the measured data to the angles of attack and flow velocities.

Each cantilever produces unique calibration surfaces, which significantly depend on the cantilever's orientation and its mechanical properties. The maximum ranges are dependent on the length of the cantilever, the size of the 2d-PSD and its distance to the cantilever. A cantilever of 140 μm in length allows for a calibration in a range of 1 m s^{-1} to at least 50 m s^{-1} (the maximum velocity of our wind tunnel). However, short cantilevers perform rather poorly at velocities of around 1 m s^{-1}. The error is about 20% for the longitudinal and 30% for the

8
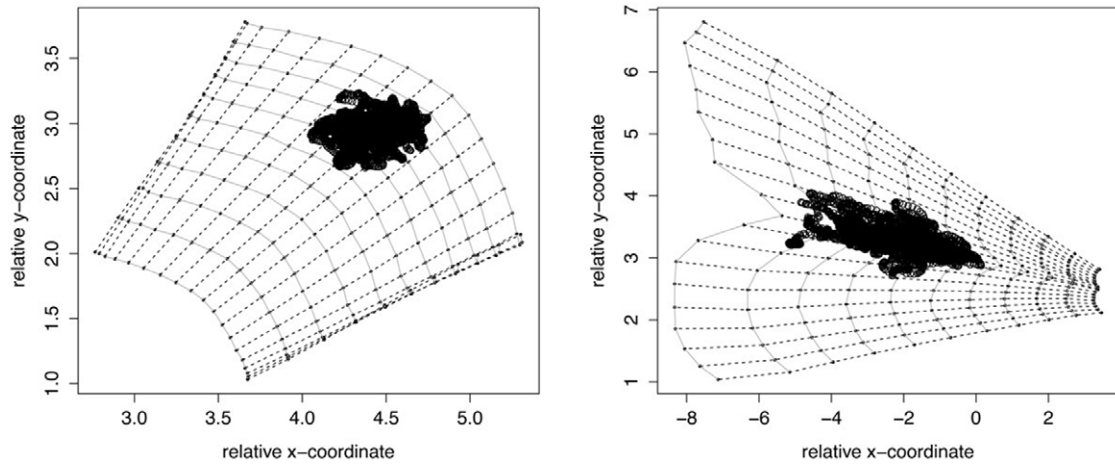
Figure 13. Calibration of the X-wire (*left*) and calibration of 2d-LCA (*right*) with 10 000 raw data points.

Table 1. Key parameters of the flow measured with the 2d-LCA and a X-wire.

| Parameter	2d-LCA	2d-LCA (averaged)	X-wire
mean velocity [m s^{-1}]	11.59 ± 0.03	11.59 ± 0.03	11.53 ± 0.03
mean angle of attack [°]	0.27 ± 0.07	0.27 ± 0.07	-0.10 ± 0.03
integral length [mm]	79.25 ± 0.23	79.81 ± 0.23	58.80 ± 0.23
Taylor length [mm]	1.48 ± 0.04	1.69 ± 0.04	1.79 ± 0.05
turbulence intensity [%]	7.95	7.92	7.32
variance [m^2 s^{-2}]	0.85	0.84	0.71

transverse velocity component. For higher velocities of above 10 m s^{-1} the error decreases to roughly 1% for both components. Better accuracy is achieved with longer cantilevers (which are more sensitive) at the expense of the upper velocity range. This is due to the limited size of the 2d-PSD and large cantilever deflections associated with high velocities.

3. Measurements

Next, we want to show turbulence measurements to demonstrate the sensor's performance. The measurement results are meant to serve as a proof of concept and will not be analyzed in full detail.

The measurements were performed using a cantilever of 160 μm in length with a vane of 50 μm in height and a commercial standard X-wire (Dantec type P51, active wire length of 1.25 mm), which served as a reference probe. The X-wire was used in CTA-mode using a Dantec Streamline 90N10 with CTA-modules of type 90C10. The overheat ratio was set to 0.8. The turbulent flow was generated using a cylinder $D = 2$ cm in diameter. Both anemometers were aligned behind the cylinder at a distance of 22D. The flow velocity was set to 12 m s^{-1}. This corresponds to a Reynolds number of 15 800.

Before analyzing the measured data, we will take a look at the raw data from both sensors, i.e. the positions of the laser spot as voltage signals for the 2d-LCA and the voltage signals corresponding to both wires in the case of the X-wire. Plotting
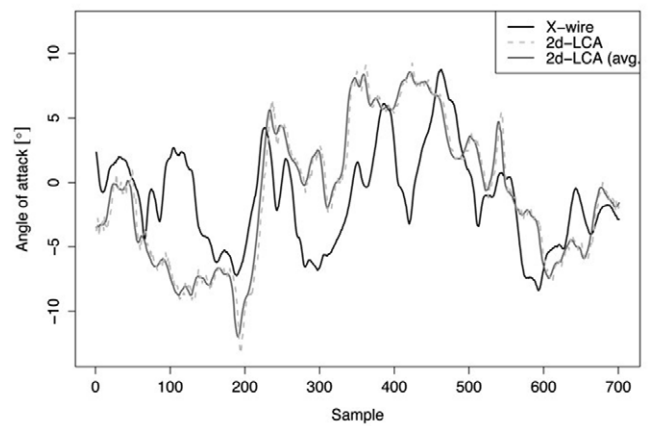

Figure 14. Time series of the measured angles of attack for the X-wire (black), the averaged 2d-LCA data (solid grey) and the original 2d-LCA data (dashed grey).

the first 10 000 points of these raw signals into the calibration planes of each sensor yields the plots shown in figure 13. Both calibration planes cover velocities from 4–14 m s^{-1} and inflow angles of $-45°$ to $+45°$.

As can be seen, in comparison to the X-wire the raw data points of the 2d-LCA are a little bit more scattered over the calibration plane. Still, all the data points of both anemometers are within the limits of the calibrated areas. We believe that this higher scattering of the 2d-LCA data is caused by the great spatial difference between both sensors. Therefore, for a more in-depth investigation we will also consider the spatially averaged 2d-LCA data, which comply with the spatial resolution of the X-wire. For this purpose, we apply a moving average over a varying number n of samples, which in sum correspond to 1.25 mm (active wire length of a Dantec P51 X-wire) when applying Taylor's hypothesis of frozen turbulence. This filter is discussed in more detail in [26].

Table 1 lists the key parameters of the flow as measured by both sensors. As can be seen the mean velocities and angles of attack agree very well for all the data sets. The values for the turbulence intensity are also very close. However, the integral length scale obtained from both 2d-LCA data sets is
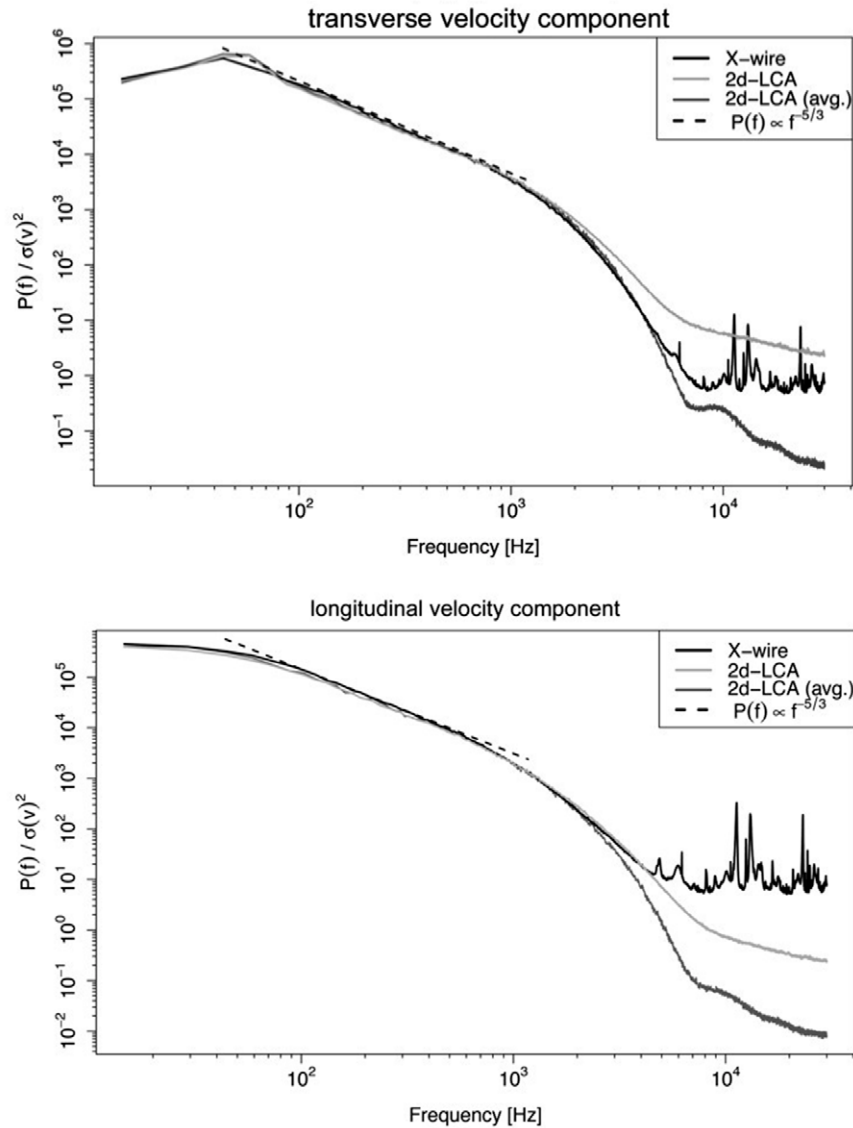
Figure 15. Power spectra of the transverse (top) and longitudinal (bottom) velocity component for the original 2d-LCA (light grey), the averaged 2d-LCA (dark grey), and the X-wire (black). The black dashed line indicates the −5/3 law according to Kolmogorov.

about 25% higher than that measured with the X-wire. The Taylor length determined from the original 2d-LCA data is the smallest with a value of 1.48 mm, whereas the averaged 2d-LCA data yield a higher value of 1.69 mm and the X-wire a value of 1.79 mm. Furthermore, the variances from both 2d-LCA data sets are slightly higher than the variance obtained from the X-wire data set. Figure 14 shows a short sequence of inflow angles as measured by both anemometers. Both time series were recorded simultaneously but at different positions within the flow. Thus, only a qualitative comparison is possible. One can see that the overall shape of the time series is very comparable.

For a more in-depth insight into the measured data, the power spectra for the longitudinal and transverse velocity component produced by both sensors are taken into account (figure 15). The black spectra correspond to the X-wire, the light-grey spectra to the original 2d-LCA and the dark-grey

spectra to the averaged 2d-LCA data. A decay according to Kolmogorov's −5/3 is indicated with a black dashed line.

The overall shapes of the original and filtered 2d-LCA spectra agree well with the X-wire spectra in the integral and inertial range for both velocity components. For higher frequencies, i.e. in the viscous subrange the spectra begin to depart from each other. For the transverse component the original 2d-LCA spectrum shows a higher energy than the X-wire spectrum, whereas the spectrum from the filtered data follows the development of the X-wire until about 4 kHz. For the longitudinal component the spectra behave in exactly the opposite way. Here, the spectrum from the original 2d-LCA data matches best with the X-wire. For both velocity components the X-wire spectra are superimposed with noise in the high frequency region.

Next, probability density functions (PDFs) of increments for various time scales τ for both velocity components are
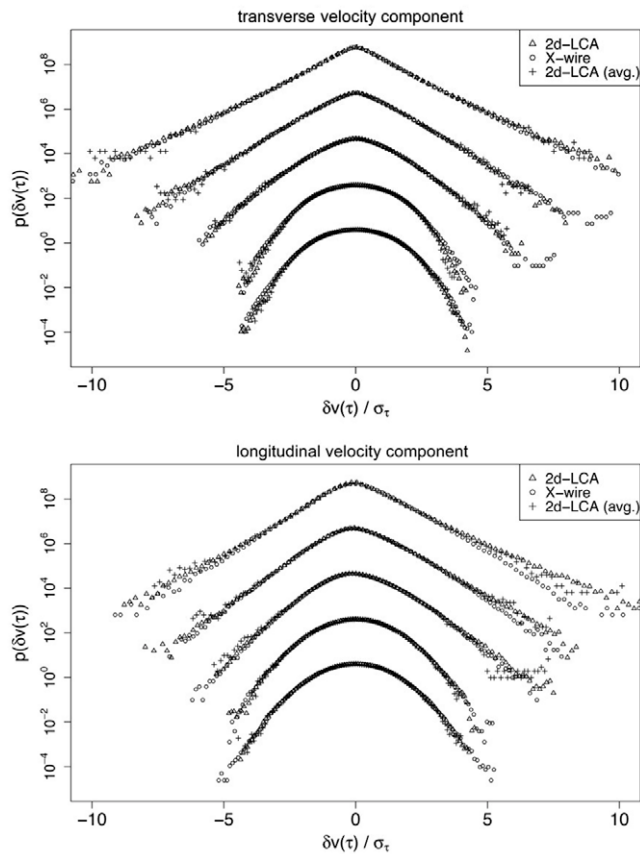
Figure 16. Probability density functions of increments for the transverse (top) and longitudinal (bottom) velocity component measured with the 2d-LCA (triangles) and the X-wire (circles). The presented time scales are (bottom to top): $\tau_1 = 3$ s, $\tau_2 = 0.33$ s, $\tau_3 = 1.7$ ms, $\tau_4 = 0.34$ ms and $\tau_5 = 0.17$ ms. For better clarity the distributions were shifted in a vertical direction by one order of magnitude against each other.

presented (figure 16). The X-wire PDFs correspond to the circles and the original and averaged 2d-LCA PDFs correspond to the triangles and crosses, respectively. The PDFs were normalized with their scale-dependent standard deviation $\sigma_\tau = \sqrt{\langle u_\tau^2 \rangle}$. The comparison shows that both anemometers reveal the same properties in the turbulent flow. In particular, the PDFs for the transverse component match very well. For the longitudinal component, both 2d-LCA datasets show a stronger pronunciation of the statistics towards larger positve increments.

4. Conclusion

The working principle of the 2d-Laser Cantilever Anemometer has been introduced and proven by means of comparative measurements with a commercial X-wire in a turbulent laboratory-generated airflow. A characterization of the sensing element, i.e. the cantilever, by means of computational and experimental methods reveals the sensors' ability to perform measurements with temporal resolutions in the range of 100 kHz. An additional vane at the tip of the cantilever improves the sensitivity towards cross winds and increases the

angular acceptance range to ± 90° relative to the cantilever. An important challenge for the future is to gain more knowledge of the cantilever's response to dynamic loads. In this regard we want to provide a precise limit for flow structures that can be detected. To date we are able to give a limit that is based on the considerations as discussed in section 2.4. According to this, structures that pass the cantilever more slowly than the time period of its first resonant mode can be fully resolved.

References

[1] Hölling M 2008 Sensorentwicklung für Turbulenzmessungen *Master Thesis* University of Oldenburg, Germany
[2] Puczylowski J 2009 Weiterentwicklung des 2D Laser-Cantilever-Anemometers *Master Thesis* University of Oldenburg, Germany
[3] Li M, Bhiladvala R, Morrow T J, Sioss J A, Lew K, Redwing J M, Keating C D and Mayer T S 2008 Bottom-up assembly of large-area nanowire resonator arrays *Nat. Nanotechnol.* **3** 88–92
[4] Barth S *et al* 2005 Laser-cantilever-anemometer: a new high resolution sensor for air and liquid flows *Rev. Sci. Instrum.* **76** 075110
[5] Örlü R, Fransson J H M and Alfredsson P H 2010 On near wall measurements of wall bounded flows: the necessity of an accurate determination of the wall position *Prog. Aerospace Sci.* **46** 353–87
[6] Janke G 1987 *Hot Wire in Wall Proximity, Advances in Turbulence* vol 1 (Berlin: Springer) pp 488–98
[7] Bhiladvala R 2012 *Nanomechanical Resonant Sensors and Fluid Interactions* (Berlin: Springer)
[8] Mullin N and Hobbs J 2008 Torsional resonance atomic force microscopy in water *Appl. Phys. Lett.* **92** 053103
[9] Lubarsky G V and Hähner G 2007 Calibration of the normal spring constant of microcantilevers in a parallel fluid flow *Rev. Sci. Instrum.* **78** 095102
[10] Manalis S R, Minne S C, Atalar A and Quate C F 1996 Interdigital cantilevers for atomic force microscopy *Appl. Phys. Lett.* **69** 3944–6
[11] Eck B 1978 *Technische Strömungslehre* (Berlin: Springer)
[12] Sigloch H 1980 *Technische Fluidmechanik* (Hannover: Schroedel)
[13] Meunier D, Tardu S, Tsamados D and Boussey J 2003 Realization and simulation of wall shear stress integrated sensors *Microelectron. J.* **34** 1129–36
[14] Naeli K and Brand O 2009 Dimensional considerations in achieving large quality factors for resonant silicon cantilevers in air *J. Appl. Phys.* **105** 014908
[15] Sader J E 1998 Frequency response of cantilever beams immersed in viscous fluids with applications to the atomic force microscope *J. Appl. Phys.* **84** 64
[16] Kampers G 2009 Charakterisierung und Optimierung der Reflexionseigenschaften von Cantilevern für die Laser-Cantilever-Anemometrie *Bachelor Thesis* University of Oldenburg, Germany
[17] Jeromin A, Schaffarczyk A, Puczylowski J, Peinke J and Hölling M 2012 Highly resolved measurements of atmospheric turbulence with the new 2d-Atmospheric Laser Cantilever Anemometer *The Science of Making Torque from Wind (Oldenburg, Germany, 2012)*

[18] Böttcher F, Barth S and Peinke J 2007 Small and large scale fluctuations in atmospheric wind speeds *Stochastic Environ. Res. Risk Assessment* **21** 299–308

[19] Tropea C, Yaris A L and Foss J F 2007 *Handbook of Experimental Fluid Mechanics* (Berlin: Springer)

[20] Bruun H H 1995 *Hot-Wire Anemometry* (Oxford: Oxford University Press)

[21] Segalini A, Örlü R, Schlatter P, Alfredsson P H, Rüedi J D and Talamelli A 2011 A method to estimate turbulence intensity and transverse Taylor microscale in turbulent flows from spatially averaged hot-wire data *Exp. Fluids* **51** 693–700

[22] Khoo B C, Chew Y T, Lim C P and Teo C J 1998 Dynamic response of a hot-wire anemometer. Part I: a marginally elevated hot-wire probe for near-wall velocity measurements *Meas. Sci. Technol.* **9** 751–63

[23] Chew Y T, Khoo B C, Lim C P and Teo C J 1998 Dynamic response of a hot-wire anemometer. Part II: a flush-mounted hot-wire and hot-film probes for wall shear stress measurements *Meas. Sci. Technol.* **9** 764–78

[24] Citriniti J H and George W K 1997 The reduction of spatial aliasing by long hot-wire anemometer probes *Exp. Fluids* **23** 217–24

[25] Ishihara T, Kaneda Y, Yokokawa M, Itakura K and Uno A 2007 Small-scale statistics in high-resolution direct numerical simulation of turbulence: Reynolds number dependence of one-point velocity gradient statistics *J. Fluid Mech.* **592** 335–66

[26] Kampers G 2012 Einfluss von unterschiedlichen Drahtlägen auf Hitzdrahtmessungen in turbulenten Strömungen *Master Thesis* University of Oldenburg, Germany